Falling Paper: Navier-Stokes Solutions, Model of Fluid Forces, and Center of Mass Elevation

Umberto Pesavento[1,*] and Z. Jane Wang[2,†]

[1]*Department of Physics, Cornell University, Ithaca, New York 14853, USA*

[2]*Theoretical and Applied Mechanics, Cornell University, Ithaca, New York 14853, USA*

(Received 28 January 2004; published 27 September 2004)

We investigate the problem of falling paper by solving the two dimensional Navier-Stokes equations subject to the motion of a free-falling body at Reynolds numbers around 10^3. The aerodynamic lift on a tumbling plate is found to be dominated by the product of linear and angular velocities rather than velocity squared, as appropriate for an airfoil. This coupling between translation and rotation provides a mechanism for a brief elevation of center of mass near the cusplike turning points. The Navier-Stokes solutions further provide the missing quantity in the classical theory of lift, the instantaneous circulation, and suggest a revised model for the fluid forces.

DOI: 10.1103/PhysRevLett.93.144501 PACS numbers: 47.32.Ff, 47.85.Gj, 47.11.+j

A piece of paper or a leaf flutters and tumbles down in a seemingly unpredictable manner (see Fig. 1). This rich dynamical behavior has inspired many experimental and modeling works on falling plates [1–4] and disks [5,6], as well as observations of dispersing seeds [7]. Even before the establishment of aerodynamic theory, Maxwell offered a qualitative explanation of the correlation between the sense of rotation and the drift direction of a tumbling card [8]. More recently, Willmarth *et al.* classified dynamics at different Reynolds numbers and dimensionless moment of inertia [5]. Belmonte *et al.* further identified a dimensionless number governing the transition from fluttering to tumbling [2]. Mahadevan *et al.* observed a relation between tumbling speed and the thickness of a falling card [3]. Models based on inviscid theory [9–14] also exhibit dynamics qualitatively similar to those seen in experiments.

What appears to be lacking is a model of the fluid force and torque that is constructed and tested against experiments or computations. The force predicted by inviscid theory includes added mass and a lift proportional to the product of velocity and circulation [10]. An unresolved issue is the choice of the circulation around the falling object, which cannot be determined from inviscid theory. Previous models either assumed the circulation to be a constant [14] or to be linearly proportional to the translational velocity [2,9,11]. The latter is appropriate for a steady translating airfoil at a small angle of attack, as given by the celebrated Kutta-Joukowski condition which requires flow velocity to be finite at the singular trailing edge [15]. The resulting lift is quadratic in velocity. While the Kutta-Joukowski condition works remarkably well in this special case, there is no direct evidence that it holds for an object fluttering or tumbling in a fluid.

Theoretical progress is in part hindered by the lack of simultaneous measurements of instantaneous forces and flows around a falling object. Here we solve the Navier-Stokes equations for the fluid subject to the dynamics of a falling body in two dimensions. Solving the falling paper problem in the most general case, i.e., free fall of a three dimensional flexible sheet, is daunting and unrealistic at Reynolds numbers of the order of 10^3. To simplify the problem, we note that bodies of relatively large span-to-chord ratios fall essentially along a two dimensional plane [4]. In the case of a business card, the span-to-chord ratio is about 1.8, and the motion in the spanwise direction is negligible. Taking advantage of these observations we focus on a falling rigid plate in a two dimensional fluid governed by the incompressible Navier-Stokes equations. The choice of a rigid plate is convenient for numerics and for comparison against existing theories. Obtaining accurate numerical solutions in this regime turns out to be nontrivial due to the thin tip of the geometry, the moving boundary coupled to the fluid forces, and the small fluid torque. Our numerical method is based on a vorticity-stream function formulation in a conformal grid fitted to the plate [16,17]. The conformal grid concentrates points at the edges of the plate and can be mapped onto a Cartesian grid in which we discretize and solve the Navier-Stokes equations efficiently via fast Fourier transform [18]. In the mapped Cartesian grid the Navier-Stokes equations take the following form:

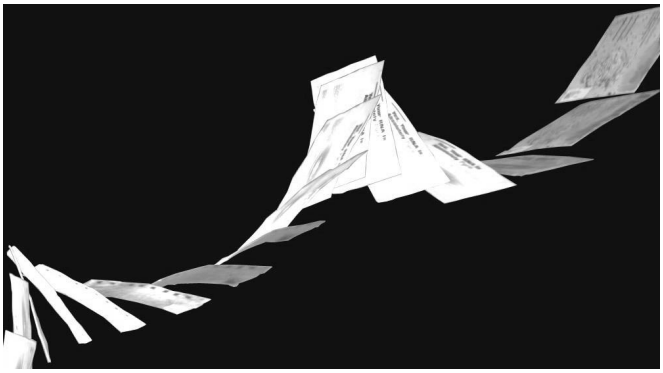

FIG. 1. Rise of a falling journal cover under windless conditions, selected frames from a footage filmed at 300 frames/s.

$$\frac{\partial(S\omega)}{\partial t} + (\sqrt{S}\mathbf{u}\cdot\nabla)\omega = \frac{1}{\mathrm{Re}}\nabla^2\omega, \tag{1}$$

$$\nabla\cdot(\sqrt{S}\mathbf{u}) = 0, \tag{2}$$

where ω and $\mathbf{u}$ are, respectively, the vorticity and velocity fields, and S is the scaling factor associated with the conformal mapping from the exterior of the plate to a semi-infinite strip. The use of body-fixed coordinates eliminates spatial interpolation as the plate moves with respect to the fluid. This turns out to be crucial for obtaining the almost periodic trajectories seen in Fig. 2. The forces on the plate are calculated by integrating the stress tensor along the body [19]. The updated velocity is then fed back to the Navier-Stokes solver through the boundary conditions. The method is applicable to arbitrary shapes of the cross section, and for simplicity, we choose an ellipse. To gauge the grid dependence of the results, we repeat simulations using grid systems of 512×1024 and 256×512 and find that the results presented below hold for both resolutions.

A falling ellipse is characterized by six parameters: the major and minor semiaxes, a and b, the densities of the ellipse, ρ_b, and of the fluid, ρ_f, the kinematic viscosity of the fluid ν, and the gravitational acceleration g [see Fig. 2(a)]. From these parameters, three dimensionless quantities can be defined: the Reynolds number, $\mathrm{Re} = 2u_t a/\nu$, using the terminal velocity estimated by balancing gravity against the fluid force on a plate of size $2a$ and drag coefficient 1, $u_t = \sqrt{\pi b g(\rho_b/\rho_f - 1)}$; the dimensionless moment of inertia, $I^* = \frac{b(a^2+b^2)\rho_b}{2a^3\rho_f}$; and the aspect ratio of the ellipse $e = b/a$. Note that the dimensionless inertia is related to the Froude number Fr defined in previous work [2], $I^* \propto \mathrm{Fr}^2$.

In Fig. 2 we show the Navier-Stokes solution of a tumbling ellipse for Re=1100, $I^* = 0.17$, and $e = 0.125$, released from rest with an initial angle of 0.2rad with respect to the horizontal. After fluttering for a short transient, the ellipse tumbles with an almost periodic motion [five periods are shown in Fig. 2(b)], which consists of gliding and quick 180° rotations. During the glide, the ellipse pitches up due to the fluid torque. The increased angle of attack results in an increased drag; thus the ellipse slows down while pitching up. The small translational velocity results in a cusplike shape near the turning points. As the plate initiates a turn, the wake becomes unstable and breaks up into vortices due to Kelvin-Helmholtz instability. The vortices have a characteristic size of half of a chord.

A casual observer of falling leaves or paper might notice that while falling downward on average, they can rise momentarily as if picked up by wind. In Fig. 1 we verify this observation by filming a falling journal cover at high speed. The case shown in Fig. 2 is an example of

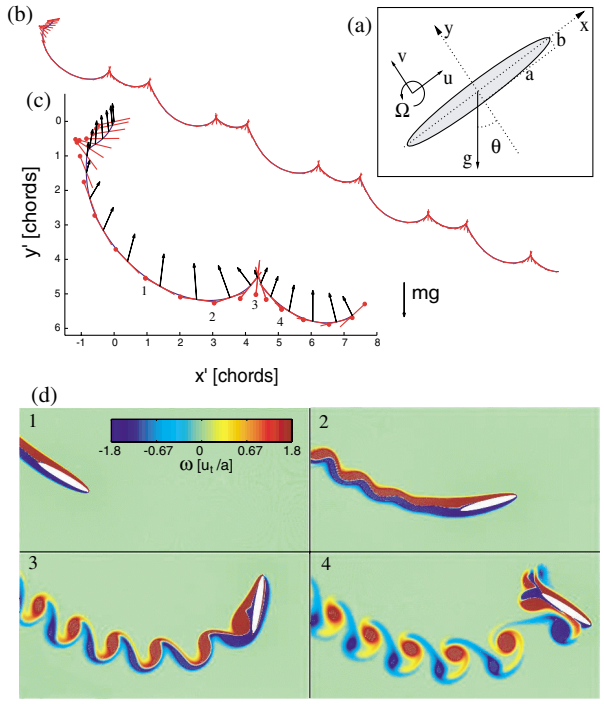

FIG. 2 (color online). Navier-Stokes solution of a tumbling ellipse at $\mathrm{Re} = 1100$, $I^* = 0.17$, and $e = 0.125$. (a) Body-fixed coordinate system and kinematic variables. (b) Trajectory and orientation of the chord (major axis of the ellipse) over five periods of motion. (c) The history of the chord and the force vector, equally spaced in time for the first period of the trajectory in (b). The chords numbered from 1 to 4 correspond to the frames shown in (d) and to the times marked with dots on the force history of Fig. 3. (d) Vorticity field at four instants during a full rotation. The frames display an area of 5×2.5 chords and they are $4a/u_t$ time units apart. The vorticity field is color coded on a logarithmic scale.

center of mass elevation for a rigid plate without ambient wind. The swinging up motion may be familiar to those who have seen sailplane stunts performing dead loops. At sufficiently high Reynolds numbers, Joukowski's theory predicts phugoid motion which swings up periodically in the special case where the angle of attack is constant and drag is negligible [9]. The situation here is different. The Reynolds number is relatively low, about 10^3, and drag is non-negligible. A straightforward modification of Joukowski's model to incorporate the lift-drag polar at Reynolds number about 10^3 predicts no center of mass elevation [20].

To investigate what might be missing in the Joukowski-like model of a falling plate, we turn to the instantaneous forces (Fig. 3). It is instructive to decompose the pressure force into the contribution of the added mass and the lift proportional to circulation, as described in inviscid theory [10,14]. The viscous force and torque F_x^ν, F_y^ν, and τ^ν are relatively small (see Fig. 3) and can be treated as perturbations. The force components, F_x and F_y, and the torque τ are defined with respect to body-fixed axes

[see Fig. 2(a)] and can be modeled as

$$F_x = -\rho_f v\Gamma + m_{12} v\Omega - m_{11}\dot{u} + (\rho_f - \rho_b)Ag\sin\theta + F_x^\nu, \tag{3}$$

$$F_y = \rho_f u\Gamma - m_{21} u\Omega - m_{22}\dot{v} + (\rho_f - \rho_b)Ag\cos\theta + F_y^\nu, \tag{4}$$

$$\tau = (m_{11} - m_{22})uv - I_a\dot{\Omega} + \tau^\nu, \tag{5}$$

where $u(t)$ and $v(t)$ are the components of the ellipse velocities along its major and minor axes, $\Omega(t)$ is its angular velocity, $\theta(t)$ is the angle between the x axis and the direction of gravity [see Fig. 2(a)], Γ is the circulation around the body, A is the area of the ellipse, m_{ij} is the components of the added mass tensor, and I_a is the added moment of inertia [15]. In the expression for the forces F_x and F_y, the first term is the lift due to the circulation around the ellipse, the second and the third terms correspond to the added mass, the fourth term is the buoyancy corrected gravity, and the F^νs are the viscous forces.

The circulation Γ is unknown and needs to be modeled to complete the equations for the pressure force. Here, we fit the pressure force from the Navier-Stokes solution by using Eqs. (3) and (4), where the added mass coefficients are left as free parameters and Γ has two contributions, one proportional to the angular velocity of the ellipse Ω and the other given by the Kutta-Joukowski condition (see Fig. 3).

$$\Gamma = c_R a^2\Omega + c_L a|\mathbf{v}|\sin(2\alpha), \tag{6}$$

where $|\mathbf{v}|$ is the speed of the ellipse and α is its angle of attack, defined as the angle between the major axis of the ellipse and its velocity vector, $\alpha \in [0, 2\pi]$.

For the falling ellipse shown in Fig. 2, the rotational contribution is about 10 times larger than the translational one. The lift corresponding to the circulation Γ is about 75% of the total lift, the remaining lift being generated by the added mass terms with coefficients m_{12} and m_{21}. It is worth noting that values m_{ij} from the force fit differ from those given by inviscid theory (see the caption of Fig. 3). Skin friction gives a contribution of about 25% of the total force and can be approximated with an expansion in the kinematic variables the ellipse u, v, and Ω (see the caption of Fig. 3). The pressure torque is 2 orders of magnitude smaller than the torque on an ellipse steadily translating with speed u_t. However, it can be modeled by a term proportional to uv as predicted by inviscid theory (see Fig. 3).

The circulation model of Eq. (6) can be validated by integrating the velocity field outside the ellipse. Figure 4 shows the circulation obtained both by fitting the pressure force with Eqs. (3) and (4) and by integrating the velocity field. The circulation displays a strong dependence on the motion of the ellipse and cannot be modeled by a constant value as in [14] or by the classical expression for a translating airfoil as in [2,11]. Instead, the circulation is better approximated by Eq. (6). The negative peaks in the circulation correspond to vortices shed at the turning points of the ellipse trajectory.

In terms of the traditional decomposition of forces into lift and drag, the proportionality between the circulation around the ellipse and its rotational velocity corresponds

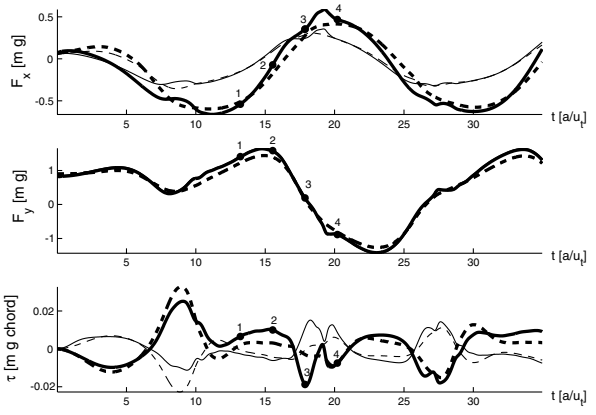

FIG. 3. The fluid force and torque on the tumbling ellipse shown in Fig. 2. Solid lines are computed forces, with the total force shown as thin lines and the pressure force as thick lines. The corresponding dashed lines are the best fits of the data based on the quasisteady model of Eqs. (3)–(5). The added mass tensor $m_{11} = 0.53m$ and $m_{12} = 3.1m$, $m_{22} = 1.5m$, $m_{21} = 0.56m$, and the circulation around the ellipse $\Gamma = 2.6a^2\Omega + 0.49a|\mathbf{v}|\sin(2\alpha)$ are obtained from the pressure force. These m_{ij} differ from those predicted by inviscid theory ($m_{11}^{\text{inv}} = m_{21}^{\text{inv}} = 0.0491m$ and $m_{22}^{\text{inv}} = m_{12}^{\text{inv}} = 3.14m$). The viscous corrections are modeled with the expansions $F_x^\nu = -\nu_{11}u - \nu_{12}u^2$, $F_y^\nu = -\nu_{21}v - \nu_{22}v^2$, and $\tau^\nu = \nu_{31}uv - \nu_{32}\Omega - \nu_{33}\Omega|\Omega|$, with $\nu_{11} = 0.18$, $\nu_{12} = 0.0075$, $\nu_{21} = 0.070$, $\nu_{22} = 0.054$, $\nu_{31} = -0.31$, $\nu_{32} = -0.05$, and $\nu_{33} = 0.16$.

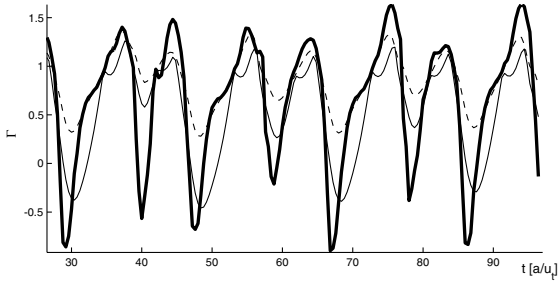

FIG. 4. Circulation as a function of time for the falling ellipse of Fig. 2. The thick line corresponds to the value of the circulation found by integrating the vorticity field up to a radius of 3/2 chords from the center of the ellipse. The thin line corresponds to the circulation obtained from fitting the pressure forces, the dashed line to the contribution of the rotational term of Eq. (6) alone. The peaks of negative circulation not captured by the fit correspond to the vortices shed by the ellipse at the turning points of its trajectory.

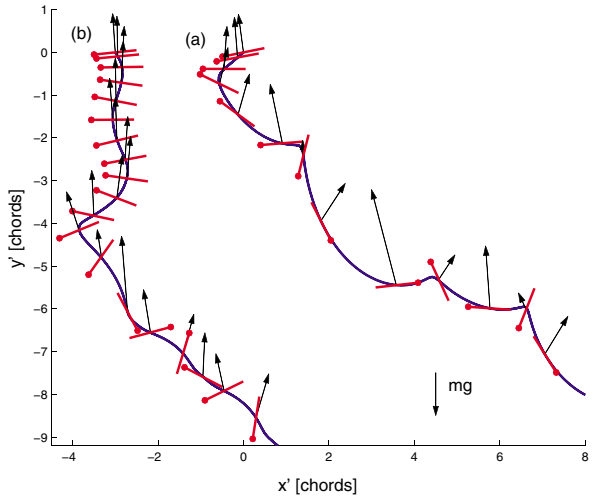

FIG. 5 (color online). Trajectories obtained from ordinary differential Eqs. (3)–(5) for different values of the translational and rotational lift coefficients c_L and c_R: (a) $c_R = 2.6$, $c_L = 0.49$, from the fit of Fig. 3; (b) $c_R = 0$, $c_L = 1.5$, as in classical translational lift. Center of mass elevation occurs in (a) but is absent in (b).

to a lift proportional to $\Omega|\mathbf{v}|$ instead of $|\mathbf{v}|^2$ as in the case of a translating plate. In the classical context, $\Omega|\mathbf{v}|$ is the predicted lift for an airfoil translating and pitching at small amplitude [21]. This is particularly important at the turning points of the trajectory, where the translational velocity is small. There, the increased angular velocity Ω compensates for the decreasing velocity $|\mathbf{v}|$ and the lift generated is sufficient for the center of mass of the ellipse to elevate. This mechanism for lift augmentation has been recently emphasized in insect hovering [22].

To further verify the connection between center of mass elevation and rotational lift, we arbitrarily vary the coefficients of the rotational and translational contributions in Eq. (6). The tumbling trajectories obtained with such a procedure are shown in Fig. 5. Models without rotational lift display center of mass elevation only for unphysical values of the lift coefficient ($c_L > 7$). On the other hand, models including rotational lift show center of mass elevation for the coefficients obtained from Navier-Stokes solutions ($c_L = 0.49$ and $c_R = 2.6$ in the case shown in Fig. 5).

Finally the flow-induced coupling between translation and rotation can decrease the speed of descent. The tumbling ellipse shown in Fig. 2 has an average descent speed of $0.4u_t$. In contrast, an identical ellipse parachuting down with its major axis perpendicular to the direction of motion would reach a terminal velocity of $0.77u_t$. It would be interesting to find out whether the slow descent and the stable direction of tumbling motion are exploited by nature, for example, in seed dispersion.

In our current work we are further validating the model presented in this Letter experimentally and using it to address the nature of the transition between fluttering and tumbling [23]. Understanding free-falling bodies might also have interesting applications to insect flight, an area of research that partly motivated this study. Although insects might take advantage of both active and passive mechanisms to control their flapping wings, only prescribed motions have been considered so far [24,25]. Falling paper is a beautiful example of a passive flight. We hope that the model presented here will be also relevant to descriptions of forces in general flapping motion.

We wish to thank M. Salganick for discussion at the early stage of this work and A. Andersen for discussion of the ODE model. This work is supported by NSF, by ONR, by AFSOR, and by Packard Foundation.

*Electronic address: up22@cornell.edu
†Electronic address: jane.wang@cornell.edu

[1] P. Dupleich, NACA Technical Report No. 1201, 1941.
[2] A. Belmonte, H. Eisenberg, and E. Moses, Phys. Rev. Lett. **81**, 345 (1998).
[3] L. Mahadevan, W. S. Ryu, and A. D. Samuel, Phys. Fluids **11**, 1 (1999).
[4] H. J. Lugt, Annu. Rev. Fluid Mech. **15**, 123 (1983).
[5] W.W. Willmarth, N. E. Hawk, and R. L. Harvey, Phys. Fluids **7**, 197 (1964).
[6] S. Field, M. Klaus, M. Moore, and F. Nori, Nature (London) **387**, 252 (1997).
[7] C. K. Augspurger, Am. J. Bot. **73**, 353 (1986).
[8] J. C. Maxwell, in *The Scientific Papers of James Clerk Maxwell* (Dover, New York, 1890), pp. 115–118.
[9] A. A. Andronov, A. A. Vitt, and S. E. Khaikin, *Theory of Oscillators* (Dover, New York, 1966).
[10] H. Lamb, *Hydrodynamics* (Dover, New York, 1945).
[11] Y. Tanabe and K. Kaneko, Phys. Rev. Lett. **73**, 1372 (1994).
[12] L. Mahadevan, H. Aref, and S.W. Jones, Phys. Rev. Lett. **75**, 1420 (1995).
[13] Y. Tanabe and K. Kaneko, Phys. Rev. Lett. **75**, 1421 (1995).
[14] L. Mahadevan, C. R. Acad. Sci. Paris **323**, 729 (1996).
[15] G. K. Batchelor, *An Introduction to Fluid Dynamics* (Cambridge University Press, Cambridge, 1967).
[16] Z. J. Wang, J. Fluid Mech. **410**, 323 (2000).
[17] Z. J. Wang, J. M. Birch, and M. H. Dickinson, J. Exp. Biol. **207**, 449 (2004).
[18] W. E and J. G. Liu, J. Comput. Phys. **126**, 122 (1996).
[19] H. J. Lugt and H. J. Haussling, J. Fluid Mech. **65**, 711 (1974).
[20] M. Salganik and Z. J. Wang (unpublished).
[21] M. M. Munk, NACA Technical Report No. 217, 1925.
[22] M. H. Dickinson, F. O. Lehmann, and S. P. Sane, Science **284**, 1954 (1999).
[23] A. Andersen, U. Pesavento, and Z. J. Wang (to be published).
[24] S. P. Sane, J. Exp. Biol. **206**, 4191 (2003).
[25] Z. J. Wang, Annu. Rev. Fluid Mech. (to be published).